12-2018

Assessing Ground Penetrating Radar's Ability to Image Subsurface Characteristics of Icy Debris Fans in Alaska and New Zealand

Robert W. Jacob
Bucknell University, rob.jacob@bucknell.edu

Jeffrey M. Trop
Bucknell University, jtrop@bucknell.edu

R. Craig Kochel
Bucknell University, kochel@bucknell.edu

Assessing Ground Penetrating Radar's Ability to Image Subsurface Characteristics of Icy Debris Fans in Alaska and New Zealand

Robert W. Jacob [1*], Jeffery M. Trop [1], and R. Craig Kochel [1]
[1] Department of Geology and Environmental Geosciences
Bucknell University, Lewisburg, PA
*Corresponding author: rob.jacob AT bucknell.edu (email), 570-577-1791 (telephone)

Accepted for publication in Journal of Environmental & Engineering Geophysics, December 2018

Abstract

Icy debris fans have recently been described as fan shaped depositional landforms associated with (or formed during) deglaciation, however, the subsurface characteristics remain essentially undocumented. We used ground penetrating radar (GPR) to non-invasively investigate the subsurface characteristics of icy debris fans (IDFs) at McCarthy Glacier, Alaska, USA and at La Perouse Glacier, South Island of New Zealand. IDFs are largely unexplored paraglacial landforms in deglaciating alpine regions at the mouths of bedrock catchments between valley glaciers and icecaps. IDFs receive deposits of mainly ice and minor lithic material through different mass-flow processes, chiefly ice avalanche and to a lesser extent debris flow, slushflow, and rockfall. We report here on the GPR signal velocity observed from 15 different wide-angle reflection/refraction (WARR) soundings on the IDFs and on the McCarthy Glacier; the effect of GPR antenna orientation relative to subsurface reflections; the effect of spreading direction of the WARR soundings relative to topographic contour; observed differences between transverse electric (TE) and transverse magnetic (TM) antenna polarization; and a GPR profile extending from the McCarthy Glacier onto an IDF. Evaluation of the WARR soundings indicates that the IDF deposits have a GPR signal velocity that is similar to the underlying glacier, and that the antenna polarization and orientation did not prevent identification of GPR reflections. The GPR profile on the McCarthy Glacier indicates that the shallowest material is layered, decreases in thickness down fan, and has evidence of brittle failure planes (crevasses). The GPR profile and WARR soundings collected in 2013 indicate that the thickness of the McCarthy Glacier is 82 m in the approximate middle of the cirque and that the IDF deposits transition with depth into flowing glacial ice.

Index Terms— ground penetrating radar, GPR, icy debris fan architecture, wide angle reflection refraction soundings.

Introduction

Icy debris fans (IDFs) may be found at the head of or along the margins of valley glaciers where high-level ice caps are detached from the valley glacier (Kochel and Trop, 2008 & 2012). The subsurface characteristics of IDFs are largely unexplored. The surface processes building these features have been observed to include ice avalanches, rockfalls, icy debris flows, and slushflows/slush avalanches (Kochel and Trop, 2012; Kochel et al., 2018), which results in a subsurface composition including snow, ice, water, air, and lithic material. These deposits can occur frequently, as much as 30 times in a single day, and can accumulate over a year to >50% of the fan volume for ice and lithic material (Kochel et al., 2018). Recent deposits on IDFs are hundreds of meters long, tens of meters wide, and meters thick (Kochel and Trop, 2012) and compact through ablation processes after deposition and to a lesser extent new deposits on top of older deposits (Kochel et al., 2018). Ice avalanches dominate IDF depositional processes; have only a small percentage of lithic material. Periods of intense ablation (or debris flow/rockfall) deposit more significant concentrations of lithic deposits (Kochel et al., 2018). Observations from exposed cross-sections within crevasses reveal that the accumulated material on the IDF contributes to the associated valley glacier (Kochel and Trop, 2012) and has been estimated to be up to 20% of glacier volume per year for one valley glacier (Kochel et al., 2018).

Subsurface structure of ice dominated features, such as glaciers, has routinely been completed using ground penetrating radar (GPR) data (e.g. Fischer and Kuhn, 2013; Rignot et al., 2013; or see Arcone, 2008; Woodward and Burke, 2007; as example review articles). GPR soundings or wide angle reflection/refraction (WARR) surveys have been used to estimate differences in GPR signal velocities to indicate changes in material, for example compaction of ice (Bradford et al., 2009). Nobes (1999) investigated GPR signal velocity anisotropy from ice-crystal alignment due to ice flow direction in glacial ice and concludes that the antenna orientation is an important design parameter. In addition, objects in the subsurface have been shown to have different GPR reflection amplitude depending on antenna polarization (Roberts and Daniels, 1998) and thus should be considered prior to collecting GPR data. The only publication of GPR data on a documented IDF prior to the present study is a limited GPR survey, consisting of only four profiles with a time window of 437 ns, which provides the only subsurface information available for IDFs (Kochel and Trop, 2008 & 2012).

We report here on the results from two IDFs located on the McCarthy Glacier, Alaska, USA (Fig. 1) and two IDFs on the La Perouse Glacier, South Island in New Zealand (Fig. 2). This work is a portion of a larger project collecting data on multiple fans in Alaska and New Zealand, as well as evaluating the prevalence and dynamic nature of these features around the world. We evaluated the effect antenna polarization had on our ability to identify reflections using a repeat GPR profile. In addition, we collected GPR WARR sounding surveys at these locations to determine the variability of GPR signal velocity within the subsurface of IDFs and relative to potential ice flow directions. We detail the results of the evaluation process here and conclude by presenting and analyzing a GPR profile extending from the McCarthy Glacier up onto an IDF.

Planned publication in JEEG, December 2018, Volume 23, Issue 4

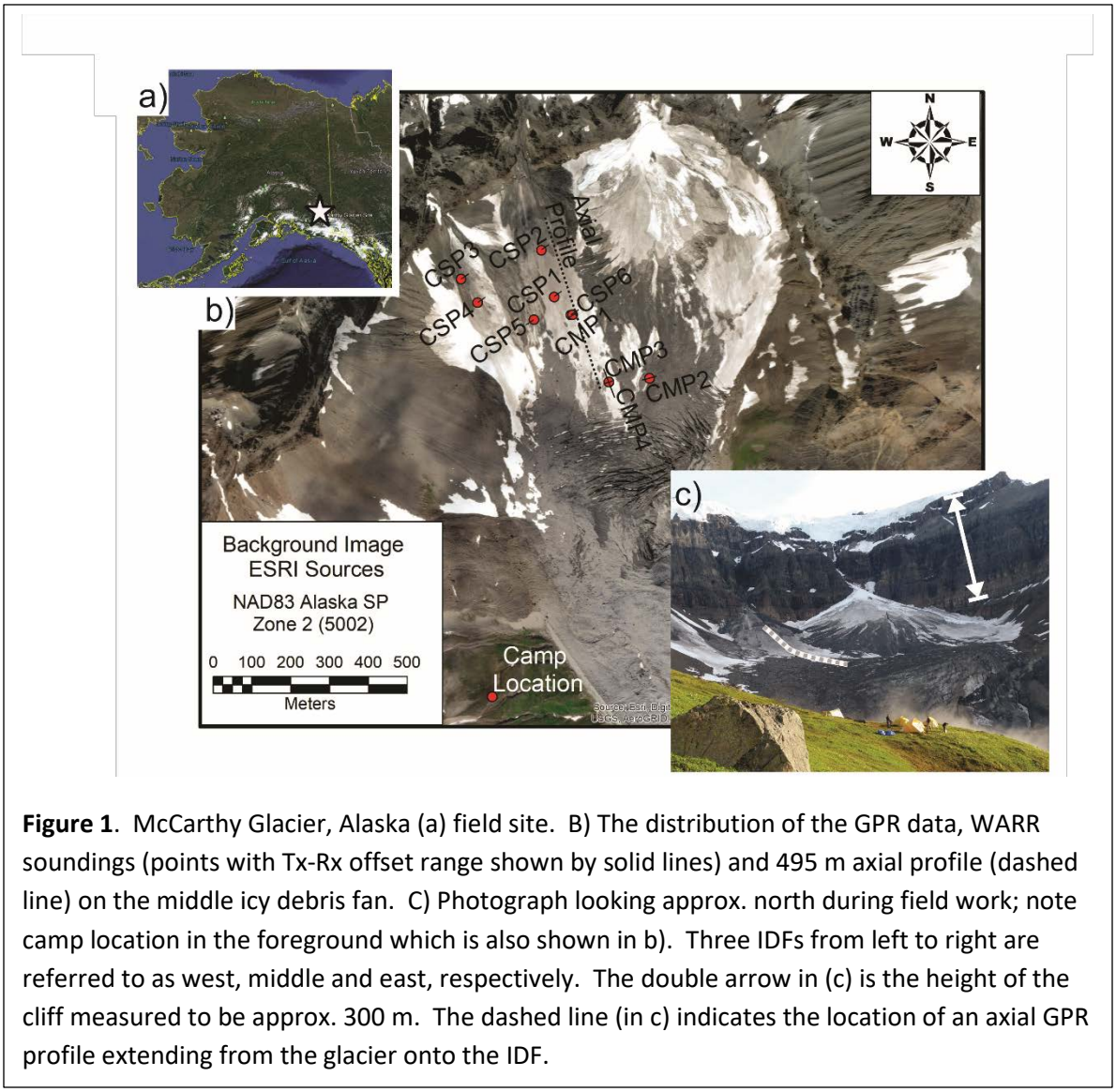

Figure 1. McCarthy Glacier, Alaska (a) field site. B) The distribution of the GPR data, WARR soundings (points with Tx-Rx offset range shown by solid lines) and 495 m axial profile (dashed line) on the middle icy debris fan. C) Photograph looking approx. north during field work; note camp location in the foreground which is also shown in b). Three IDFs from left to right are referred to as west, middle and east, respectively. The double arrow in (c) is the height of the cliff measured to be approx. 300 m. The dashed line (in c) indicates the location of an axial GPR profile extending from the glacier onto the IDF.

Methods

Data Collection

We used a Sensor & Software Pulse EKKO Pro system employing 100 MHz and 200 MHz bi-static unshielded antennas to collect multiple WARR soundings and three GPR profiles. The sample rate depended on the frequency of the antenna; 100 MHz data were sampled every 0.8 ns, while 200 MHz data were sampled every 0.4 ns. All GPR data were collected with an internal 16-fold stack per trace and a time window of 3000 ns. A Trimble R8 Model 3 real time kinematic (RTK) GPS system with two receivers (rover and base) provided horizontal and vertical position for all GPR data. The GPS base station receiver collected stationary GPS data which was corrected and referenced to either the US National Geodetic Survey's Online Positioning User Service (OPUS) for the Alaska IDFs or the Australian Positional Service network (AUSPOS) for the New Zealand IDFs. The GPS positioning has horizontal precisions of <0.1 m and vertical precisions of < 0.15 m for all GPR data.

Planned publication in JEEG, December 2018, Volume 23, Issue 4

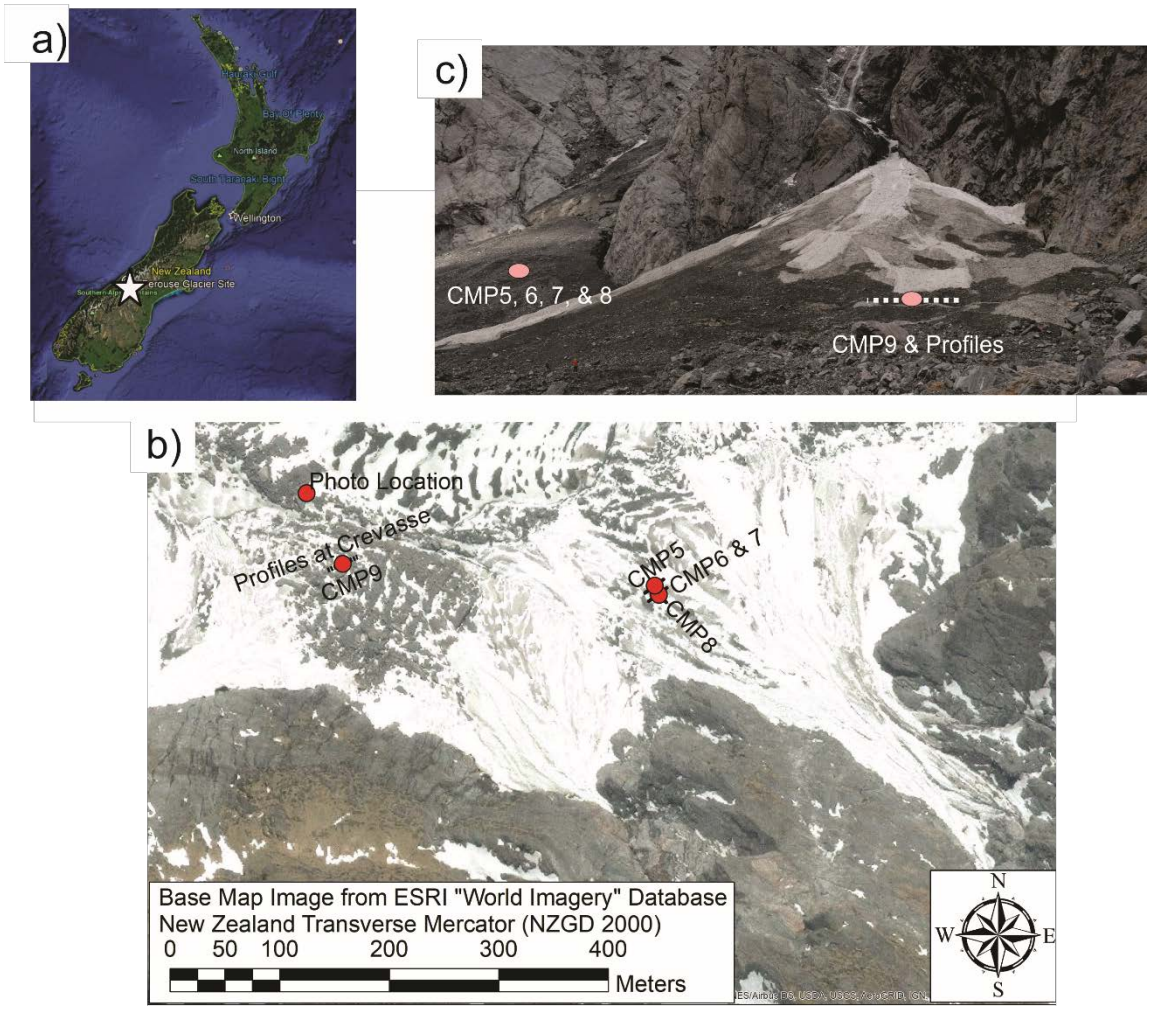

Figure 2. La Perouse Glacier, New Zealand (a) field site. B) The distribution of the GPR data, CMP soundings (points with Tx-Rx offset range shown by solid lines) and repeated profiles 2 m south of a crevasse (dashed line) on the middle icy debris fan. C) Photograph looking approx. south, note photo location shown in b) on the La Perouse Glacier, not from the same date as 2014 CMP soundings. The two IDFs in the photograph (c) from left to right are referred to as east and middle, respectively. The gray dashed line (c) indicates the location of two repeated GPR profiles on the low portion of the middle icy debris fan adjacent to a crevasse. The circles (c) provide approx. locations of the CMP soundings shown in (b).

The WARR soundings were collected as either common shot-point (CSP) or common mid-point (CMP) configurations [see Annan, 2005 for details on these configurations] at both glacier sites, on four different IDFs, and at different locations on each IDF as indicated in Table 1 and Fig. 1b and Fig. 2b. The decision to collect CSP vs. CMP soundings was based on available field personnel, as a CMP required at least two operators on the icy surface. We collected WARR soundings in both transverse electric (TE) polarization [also referred to as broadside (Annan, 2005)] and transverse magnetic (TM) polarization [also referred to as end-fire]. The orientation of the spreading axis for each WARR sounding was either

parallel to topographic contours on the IDF surface [referred to as transverse] or perpendicular to the contour of the IDF surface [referred to as axial]. Each WARR sounding was collected using a tape measure to provide distance control and either the "shot" point or mid-point locations were located with the RTK-GPS. The offset range for the transmitter (Tx) to receiver (Rx) separation varied, starting at 1 m offset and commonly limited to 20 m but one CMP had a total Tx-Rx offset of 80 m (Table 1). All WARR soundings increased their Tx-Rx offset by 0.2 m except CMP3, where the offsets between 20 m and 80 m had a 0.5 m step size. We maintained the Tx-Rx offset step-size of CMP3 between 1 and 20 m in order to have optimal step-size for the 100 MHz antennas for the shallow reflections. Meanwhile, the larger offsets were collected for the deeper reflections where we chose to increase the step-size to maximize the amount of GPR data collected over the entire IDF in our fixed amount of field time by minimizing time required for this single WARR sounding.

Table 1. WARR sounding information for icy debris fan sites. Spread orientation is relative to the slope of the icy debris fans (IDFs), where transverse is along a contour line on the IDF and axial is perpendicular to the contour of the IDF surface. Date is month/day.

WARR name & configuration	Site	IDF at site or on glacier	Position on fan	Year	Date	Frequency (MHz)	Polarization	Spread orientation	Offset range (m)
CSP1	McCarthy	Middle	Low	2013	07/13	100	TE	Transverse	1 to 18
CSP2	McCarthy	Middle	Mid	2013	07/13	100	TE	Transverse	1 to 19
CSP3	McCarthy	West	Mid	2013	07/13	100	TE	Transverse	1 to 19
CSP4	McCarthy	West	Low	2013	07/13	100	TE	Transverse	1 to 19
CSP5	McCarthy	West	Toe	2013	07/14	100	TE	Transverse	1 to 20
CSP6	McCarthy	Middle	Toe	2013	07/14	100	TE	Transverse	1 to 20
CMP1	McCarthy	Middle	Toe	2013	07/14	100	TE	Transverse	1 to 36
CMP2	McCarthy	Glacier	Off Fan	2013	07/14	100	TE	Transverse	1 to 30
CMP3	McCarthy	Glacier	Off Fan	2015	06/23	100	TE	Axial	1 to 80
CMP4	McCarthy	Glacier	Off Fan	2015	06/23	100	TE	Transverse	1 to 20
CMP5	La Perouse	East	Mid	2014	03/09	200	TE	Transverse	1 to 20
CMP6	La Perouse	East	Mid	2014	03/13	100	TE	Transverse	1 to 20
CMP7	La Perouse	East	Mid	2014	03/13	100	TM	Transverse	1 to 20
CMP8	La Perouse	East	Mid	2014	03/13	100	TE	Axial	1 to 20
CMP9	La Perouse	Middle	Low	2015	03/11	100	TE	Transverse	1 to 21

Planned publication in JEEG, December 2018, Volume 23, Issue 4

WARR soundings that expand about the same mid-points (Fig. 1b and Fig. 2b) were collected to evaluate different variations in our data collection procedure. Specifically, CMP1 was collected in the middle of CSP6 (Fig. 1b) in order to evaluate if the WARR sounding configuration affected the observed GPR signal velocity. CMP3 and CMP4 (Fig. 1b) shared a common mid-point but the spreading direction was perpendicular, where CMP3 offsets in a N-S orientation – approximately parallel to glacial flow axis – and CMP4 offsets increased in a E-W orientation. The mid-point of CMP5 (Fig. 2b) was collected less than 5 m away from the mid-point of CMP6 in order to evaluate effects of four days of ablation on a recent (less than 5 days old) ice avalanche deposit. CMP6, CMP7, and CMP8 (Fig. 2b) also shared a common mid-point but CMP6 was collected in TE polarization, CMP7 was collected in TM polarization, and the spreading orientation for CMP8 was perpendicular to the other two.

The antenna orientation relative to subsurface reflectors for temperate glaciers has been shown to effect GPR reflections (Nobes, 1999). In order to further evaluate any similar effect on GPR data collected on IDFs, we collected two 100 MHz GPR profiles with a one-meter Tx-Rx offset and a step size of 0.25 m along the same line on the middle La Perouse fan (Fig. 2b), one with GPR antenna orientation being parallel broadside and the other having antenna orientation of perpendicular broadside [see Annan, 2005 for definition]. The location for this profile line was two meters away from an open crevasse in the fan exposing subsurface interfaces. Additionally, at the center of this profile line, we collected a CMP sounding (CMP9) as a Quality Control / Quality Assurance procedure to allow comparisons between the visible subsurface stratigraphy and the GPR reflections.

We collected a 495 m long GPR profile shown in Fig. 1b (dashed line) at McCarthy Glacier site extending from the glacier up onto the middle IDF. The GPR profile was collected using the 100 MHz unshielded bistatic antennas in broadside configuration with a Tx-Rx offset of 1 m and a nominal 0.5 m step size measured using markings on the antennas and the GPS data.

Data Processing

The GPR data processing of the WARR surveys initiated with correcting the time-zero at zero-offset of the first-break of the direct air phase to zero time. The GPR velocity of the direct air phase for all WARR survey data indicated that no time-base correction was necessary (Jacob and Hermance, 2005). Initial GPR data processing for profile surveys also corrected the time-zero at zero-offset of the first-break of the direct air phase.

The GPR processing continued, using EKKO Project from Sensor & Software, Inc., however, any number of commercially available software or in-house software could provide the same processing. The WARR data were then dewowed with no other spatial or temporal filtering applied. Constant gains were applied for WARR data presentation. The profile data processing included dewow and minimal gain. The 495 m long GPR profile had the average background trace subtracted from each trace, and was topographically corrected using the GPS elevation data and the appropriate GPR velocity from associated WARR data. The 495 m long profile was migrated using a 2D FFT Stolt migration operator (Sensors & Software, Inc., 2015) using the same GPR velocity from topographic correction.

Data Analysis

Semblance analysis using EKKO Project provided the GPR signal velocity as normal moveout (NMO) velocity and two-way traveltime at zero-offset (TWTT) for the observed reflector(s) from the WARR soundings. The NMO velocity based on the peak semblance pick is not necessarily the best estimate of electromagnetic signal velocity through a material (Booth et al., 2010), however, picking the peak of the semblance analysis provides an efficient method to determine NMO velocity (Jacob and Urban, 2016) with minimal error for depth estimates as well as for the antenna frequencies in this report (Murray et al., 2007).

Results

The results of the semblance analysis for the WARR soundings from the McCarthy IDFs are presented in Table 2. An example analysis of a WARR sounding (CSP1) and associated semblance plot are presented as Fig. 3. The radargram from CSP1 (Fig. 3a) is representative of the CSP soundings collected in this study, where in addition to the GPR events (or phases) that display an increase in arrival time with increasing distance, there are several GPR events that appear to decrease their traveltime as Tx-Rx offset increases. The NMO velocity for CSP1 does not change significantly with depth, notice that the peak semblance amplitudes in Fig. 3b occur between 0.15 and 0.16 m/ns to a TWTT of 315 ns. The NMO velocity on these IDFs varies between 0.150 and 0.172 m/ns, however, most of these NMO velocity estimates are less than 0.161 m/ns. The median velocity is 0.156 m/ns. We note that two of the velocities above 0.17 m/ns occur on the West IDF. There is a difference of 0.011 m/ns in NMO velocity between the reflected phase at a TWTT of 585 from CSP6 compared to the reflected phase at a TWTT of 568 from CMP1, even though the mid-point of CMP1 was located at the center of the Tx-Rx offsets of CSP6, i.e. 10 m from the “shot” point of CSP6. The deepest reflected phase in CMP1 at a TWTT of 1048 ns was not observed in CSP6.

Table 2. Velocity analysis results from WARR soundings at the icy debris fans on McCarthy Glacier, Alaska.

WARR name	Reflected phase 1		Reflected phase 2		Reflected phase 3	
	NMO velocity (m/ns)	TWTT (ns)	NMO velocity (m/ns)	TWTT (ns)	NMO velocity (m/ns)	TWTT (ns)
CSP1	0.153	12	0.155	55	0.156	315.37
CSP2	0.155	12.3	0.155	44.1	0.158	435.3
CSP3	0.171	54				
CSP4	0.172	62	0.155	184		
CSP5	0.161	42				
CSP6	0.163	25	0.150	585		
CMP1	0.161	29.7	0.161	568	0.155	1048

Planned publication in JEEG, December 2018, Volume 23, Issue 4

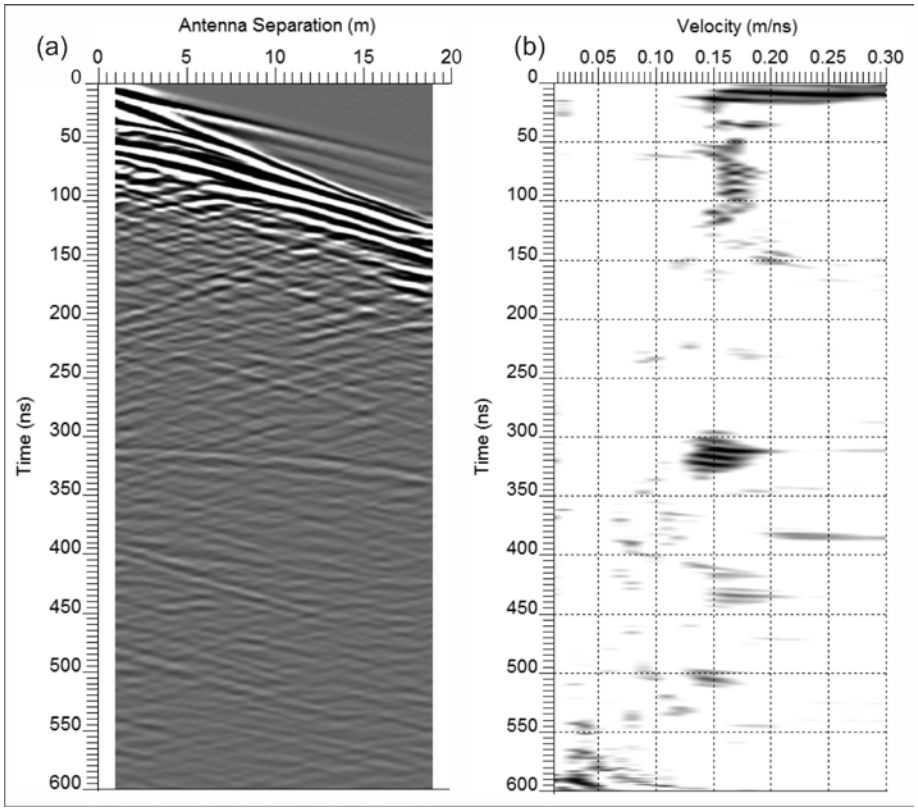

Figure 3. WARR sounding (a) and semblance analysis (b) of CSP1 (Table 1) collected on the icy debris fan approximately 20 m west of the dashed line in Figure 1 from the McCarthy Glacier site in Alaska. GPR sounding data are dewowed and have a constant gain applied. Velocity analysis results provided

Table 3 presents the velocity analysis results from the La Perouse IDFs and Fig. 4 presents an example of a WARR sounding (CMP9) and associated semblance plot. The peak semblance amplitudes

Table 3. Velocity analysis results from WARR soundings at the icy debris fans on La Perouse Glacier, New Zealand. CMP6, CMP7, and CMP8 were collected at the same mid-point on a recent ice avalanche deposit.

WARR Name	Reflected phase 1		Reflected phase 2		Reflected phase 3		Reflected phase 4	
	NMO velocity (m/ns)	TWTT (ns)	NMO velocity (m/ns)	TWTT (ns)	NMO velocity (m/ns)	TWTT (ns)	NMO velocity (m/ns)	TWTT (ns)
CMP5	0.161	17	0.159	46				
CMP6	0.159	13.0	0.159	50.6	0.159	81	0.159	122
CMP7	0.156	15.2	0.159	48	0.159	81	0.158	127.2
CMP8	0.159	13.7	0.167	52.8	0.182	79	0.173	121
CMP9	0.158	14.1	0.174	53.4				

(Fig. 4b) indicate that the NMO velocity increases with increasing depth to a TWTT of 53 ns (from 0.158 m/ns to 0.174 m/ns). The NMO velocity on these IDFs varies between 0.158 m/ns to 0.182 m/ns with most of the NMO velocities below 0.161 m/ns. We note that the velocities above 0.161 m/ns occur on CMP8 and from CMP9. The two GPR profiles collected along the crevasse in the middle IDF at La Perouse show that there is a dipping reflector and the associated photograph of the crevasse reveals an interface that has similar slope (Fig. 5). The GPR data (Fig. 5a and 5b) are presented with minimal processing, only time-zero correction, dewow, and constant gain.

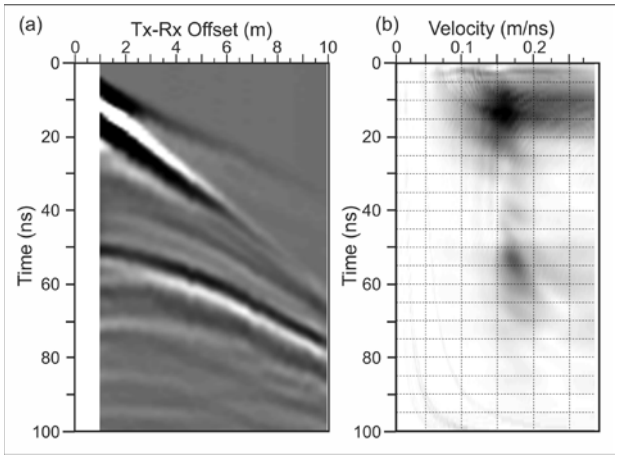

Figure 4. WARR sounding (a) and semblance analysis (b) of CMP9 (Table 1) collected on the icy debris fan along the dashed line in Figure 2 from the La Perouse Glacier site in New Zealand. GPR sounding data are dewowed and have a constant gain applied. Velocity analysis results provided in Table 3.

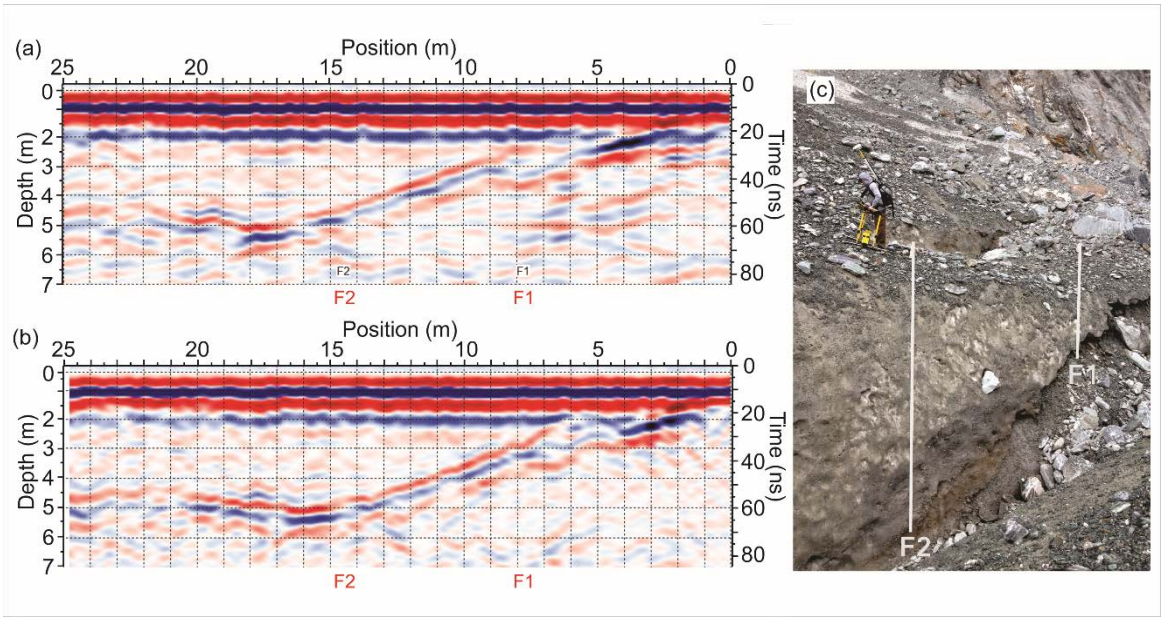

Figure 5. GPR profiles (a and b) adjacent to crevasse (c) exposing subsurface stratigraphy in icy debris fan on the La Perouse glacier (dashed line in Fig. 2). The GPR profiles were collected in broadside parallel (a) and broadside perpendicular (b) relative to the profile line, or more importantly broadside perpendicular to the axis of the fan (a) and broadside parallel to the axis of the fan (b). Both profiles have the same processing applied to them (dewow and constant gain). The fiducials (F1 & F2) in GPR profiles correlate with the vertical lines on the photograph (c). The associated CMP (CMP9 in Table 1 and presented in Figure 4) was collected with the mid-point at a position of 13 m.

Table 4 presents the results of semblance analysis from the WARR soundings collected only on the McCarthy Glacier. In addition, an example of one of these WARR soundings (CMP3) and associated semblance analysis is provided in Fig. 6. The radargram from CMP3 (Fig. 6a) is representative of the CMP soundings collected in this study, where the GPR events have either linear moveout with Tx-Rx offset, or normal moveout with Tx-Rx offset, i.e. traveltime increases as offset increases. The NMO velocity for CMP3 does not change significantly with depth, notice that the peak semblance amplitudes in Fig. 6b occur between 0.16 and 0.17 m/ns to a TWTT of 1104 ns.

Table 4. Velocity analysis results from WARR soundings on McCarthy Glacier, Alaska. CMP2 was collected near a large moulin. CMP3 and CMP4 were collected at the same mid-point.

WARR name	Reflected phase 1		Reflected phase 2	
	NMO velocity (m/ns)	TWTT (ns)	NMO velocity (m/ns)	TWTT (ns)
CMP2	0.161	105	0.125	1163
CMP3	0.164	100.9	0.161	1104.2
CMP4	0.168	101.2	0.161	1113.0

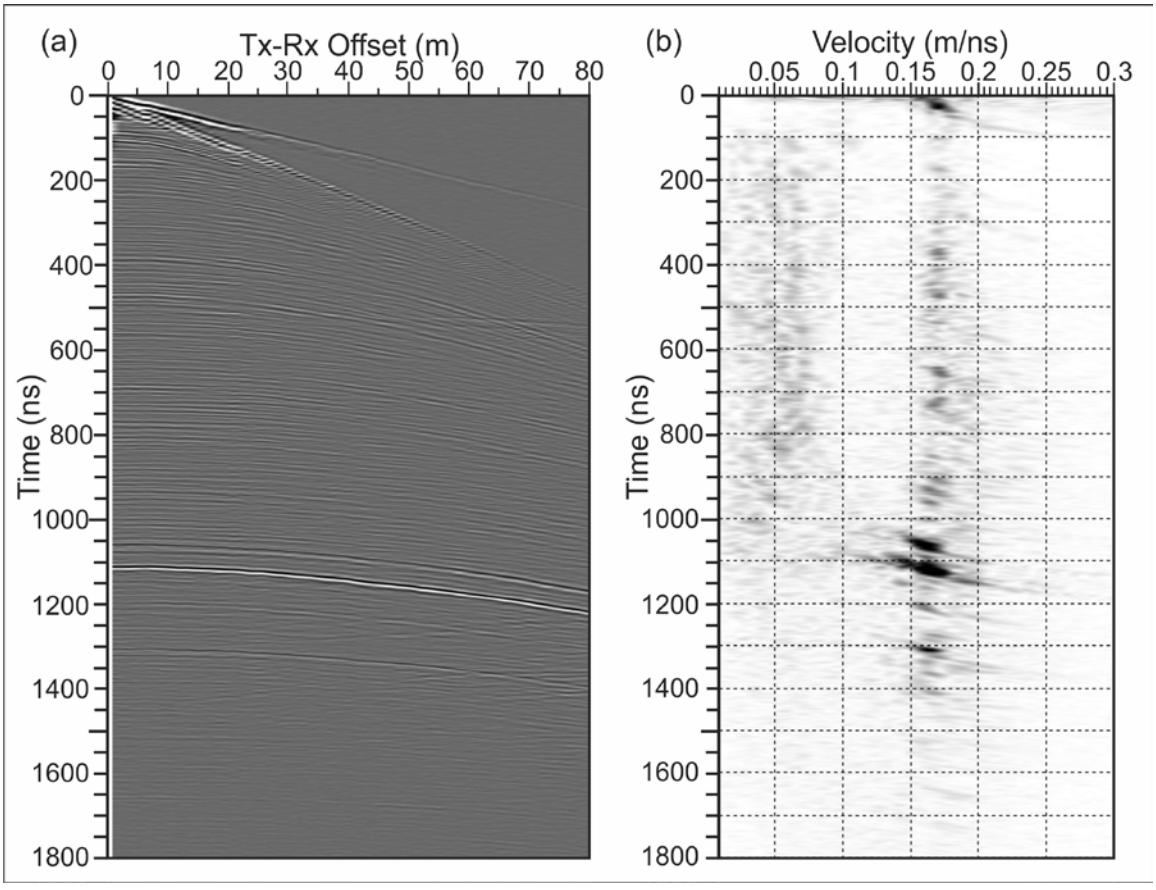

Figure 6. WARR sounding (a) and semblance analysis (b) of CMP3 (Table 1) collected on the McCarthy Glacier in Alaska about 20 m east of the dashed line in Figure 1. GPR sounding data are dewowed and have a constant gain applied. Velocity analysis results provided in Table 4.

The axial GPR profile from the middle IDF (dashed line Fig. 1) at the McCarthy Glacier field site is provided as Fig. 7. The depth provided is using the NMO velocity of 0.158 m/ns associated with the deep reflector from CSP2 (Table 2). The full 495 m long profile starting on the McCarthy Glacier and extending onto the middle IDF (dashed line Fig. 1) is provided as Fig. 8. We provide the GPR profile without migration and enlarged (Fig. 7) to illustrate interesting subsurface architecture revealed by the GPR data, whereas the topographically corrected and migrated GPR profile (Fig. 8) shows the inferred thickness of both the McCarthy Glacier and the inferred thickness below the middle IDF.

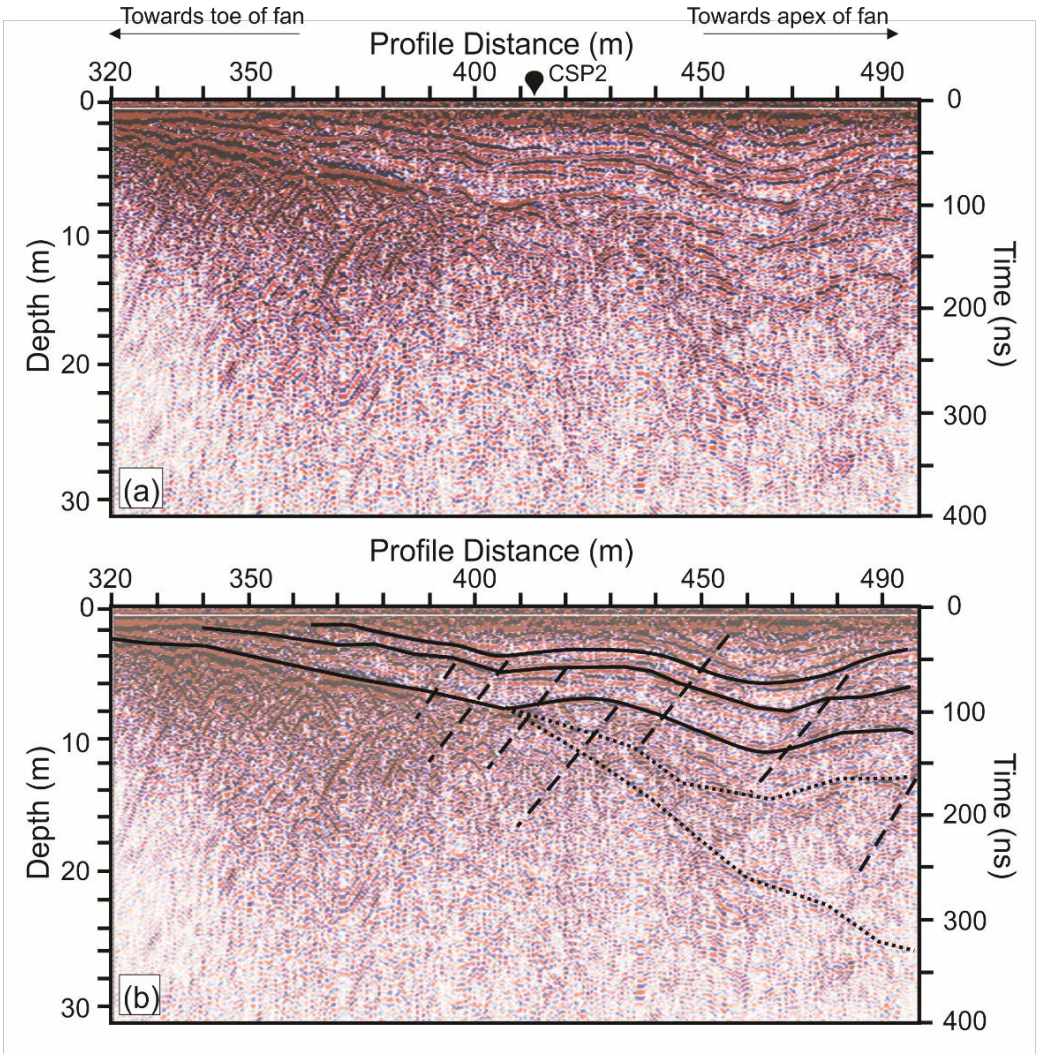

Figure 7. Axial GPR profile (a) and interpreted subsurface structure (b) of the middle icy debris fan at the McCarthy Glacier with increasing profile distance toward the fan apex (cliff) in Fig. 1. The data are dewowed and have a constant gain applied. Depth based on GPR signal velocity of 0.158 m/ns from a reflection at a TWTT of 435 ns on CSP2 (Table 2). Solid lines denote prominent layered reflections. Dashed lines indicate offsets in the prominent reflectors interpreted as faults. Below the deepest solid line, there are more abundant hyperbolic reflections interpreted as either crevasses or boulders (lithic clasts). The dotted-lines denote reflections that become less defined with depth.

Discussion

Antenna Polarization and Orientation Effects

Antenna polarization. The effects of antenna polarization (TE vs TM) on reflected signals were evaluated by comparing CMP6 and CMP7. The analysis results from the deeper reflected signals (Reflection 2, 3, and 4 in Table 3) indicate that there is little difference in velocity estimates. Furthermore, visual observations of reflections from the CMP soundings, including the deeper reflection (TWTT = 850 ns), indicate that the ability to identify these reflections is not dependent on the antenna polarization. And since GPR antennas are easier to operate by a single operator during GPR profiles, we collected the GPR data on the IDFs in the TE polarization.

Antenna orientation vs. fan axis. We compare the GPR profiles collected near the crevasse at the La Perouse IDF in Fig. 5 to evaluate the effects of antenna orientation relative to the axis of the IDF. The antenna orientation for Fig. 5a was broadside parallel, which means that the antennas were perpendicular to the fan's axis – or parallel to topographic contours. Comparing the two profiles (Fig. 5a vs 5b), there is little difference in the prominent reflector due to the orientation of the antennas. The subtle difference is between positions of 2 to 8 m and located below the primary sloping reflector, which is positioned at travel-times between 40-60 ns. This possible reflection is only observed when the antennas are perpendicular to the axis of the fan. We collect the GPR profile data with the antennas parallel to topographic contours, or perpendicular to the axis of the fan, to maximize the potential to image even subtle interfaces. In addition, standing or walking parallel to contours (including walking sideways uphill) on an IDF proved to be safer on the icy, high-gradient surface. (side note: the abundant coarse lithic content on the IDF made crampons difficult to use.)

WARR Soundings

CSP vs. CMP configurations. Comparing the results from CSP6 to CMP1, the shallow reflection has a difference of 0.002 m/ns in NMO velocity and 0.4 m in depth to the interface. This slight difference may be related the 10 m spatial shift between the small-offset location for the reflections in CSP6 versus the mid-point of CMP1 and thus indicating a small dip angle if the reflecting interface is the same. The deeper reflected phase indicates greater variation of velocity, where the reflection from a TWTT of approximately 570 ns (Reflection #2 in Table 2) is 0.150 m/ns vs. 0.161 m/ns, respectively, and a 2.7 m difference in depth. Similar to the shallow reflection, this difference may be due to an inferred dipping reflecting interface with a larger dip than the shallow interface. We would expect that the apparent velocity from a dipping interface would have higher error from the CSP configuration than the CMP configuration. These results in addition to the inability of CSP6 to image the deepest reflection observed in CMP1 (TWTT = 1048 ns) lead to CMP soundings being the preferred WARR configuration.

NMO velocity of icy debris fans. As described in the "Antenna orientation vs. fan axis" subsection, there is an observed dipping interface (Fig. 5c) below the mid-point of CMP9. Reflection #2 (Table 3) from CMP9 relates to this sloping interface, and has a NMO velocity of 0.174 m/ns. Thus this NMO velocity estimate is considered biased due to the observed dipping interface. We suspect that the

two NMO velocity estimates greater than 0.17 m/ns from CMP8 are similarly biased. CMP8 was collected with the same mid-point as CMP6 and CMP7, but the NMO velocity for the third and fourth reflected phases (Table 3) are different. The difference between CMP8 and the co-located CMPs was that the spread orientation was axial (Table 1), and suggests that the deeper reflectors (Reflected Phase 2, 3, and 4 in Table 3) were sloping relative to the icy debris fan surface which biased the velocity estimate relative to those from the co-located CMP6 or CMP7.

Removing the biased velocity estimates from CMP8 and CMP9, the median GPR velocity from all IDF reflected phases (Tables 2 and 3) is 0.159 m/ns. In future processing of GPR profile data collected in locations on the McCarthy and La Perouse IDFs that did not have a WARR sounding due to time constraints, we can use this median velocity as first attempt for migration.

The NMO velocity from the IDFs increases or remains relatively constant with depth for all WARR soundings except for the previously noted CSP soundings on the West IDF in McCarthy (CSP3 & CSP4) and CMP5 from La Perouse. Interestingly, CMP5 was collected on a recent (less than 5 days old) ice avalanche deposit with a GPR signal velocity of 0.161 m/ns. Whereas the GPR signal velocity from the same deposit (CMP6) four days later was 0.159 m/ns, for the shallowest reflection (Reflection 1 in Table 3). This decrease in GPR signal velocity corresponds to the observation that porosity decreases during compaction and ablation in these ice avalanche deposits, thus decreasing the air fraction.

NMO velocity quality control / quality assurance. In order to check our velocity analysis, we compare the depth estimated to the prominent reflection in Fig. 4 (TWTT = 53 ns) and Fig. 5a & b to the depth observed in a visible cross-section of the IDF exposed by a crevasse (Fig. 5c). The measured depth to the break in the icy material (Fig. 5c) at the position of the CMP sounding (position 13 m in Fig. 5a & b) is 4.1 m below the surface. First we check this measured depth relative to the CMP9 semblance results. As further evidence for the bias in the NMO velocity from Reflection 2 due to the sloping reflector, the GPR observed depth using the biased NMO velocity of 0.174 m/ns and the TWTT of 53.4, would indicate the depth to this reflecting interface of 4.6 m. Meanwhile, using the NMO velocity estimate from the shallower reflection, 0.158 m/ns, the depth to the reflecting interface would be 4.2 m, thus further indicating that the 0.174 m/ns velocity estimate was biased by the slope of the interface. Hence, we use the shallow-most NMO velocity (0.158 m/ns) to calculate the depth below surface for the GPR profiles. Using this velocity, there is good agreement between the GPR depth to this interface (3.9 m in Fig. 5a or 4.2 in Fig. 5b) and the depth observed in the field.

NMO velocity of McCarthy Glacier. CMP3 indicates that the NMO velocity profile is very consistent to a TWTT of 1300 ns (Fig. 6b). Although, the range in NMO velocity estimates at the McCarthy Glacier is 0.125 m/ns to 0.168 m/ns, with the median NMO velocity estimate as 0.161 m/ns. Interestingly CMP2 has the lowest NMO velocity estimate in this study, which was collected 105 m away from CMP3 / CMP4 but in close proximity to an active moulin, where at the time of data collection a constant flow of water was draining off the glacial surface into the moulin. Thus we posit that this slow NMO velocity is indicative of liquid water filling in pore space at depth. Comparing the NMO velocities between CMP3 and CMP4, which had perpendicular spreading directions, indicate that there is no

difference to the reflected phase at 90 m depth (0.161 m/ns for each), thus suggesting that there is not GPR velocity anisotropy in this part of the glacier. Interestingly, there is a greater difference in NMO velocity above the reflecting interface at 8.4 m depth, however, we cannot solely attribute this to anisotropy as there may be a dipping interface that affected the NMO velocity estimate for CMP3 and/or CMP4.

GPR Profile on McCarthy Glacier and Middle Icy Debris Fan

We use the difference in NMO velocity of the McCarthy Glacier compared to the McCarthy IDFs to evaluate and extend our understanding based on the axial profile at the McCarthy site (dashed line in Fig. 1). A section of the entire GPR profile is provided in Fig. 7, which is presented with minimal processing; time-zero correction, dewow, background average subtraction, and constant gain. There is a change in the observed GPR signal characteristics with depth below the surface of the IDF (Fig. 7). The shallow GPR reflections above a depth of 8 m at CSP2 include three prominent subparallel and laterally continuous reflectors (solid lines in Fig. 7b). These reflectors are observed to decrease in depth toward the toe of the fan (left side of Fig. 7) and thus converge by decreasing thickness of the material between reflectors. In addition, these reflections appear to be offset by high-angle features (dashed lines in Fig. 7b). We interpret these shallow GPR reflections to be layers produced by alternating episodes of aggradation of numerous ice-rich mass flow deposits followed by protracted episodes of ablation and concentration of lithic material (Kochel et al., 2018), similar to the visible boundary in Fig. 5c. These subsurface layers thin toward the toe of the IDF as distance down-fan increases, and also indicate crevasses within these layered deposits that imply vertical movement within the fan (Fig. 7b). Below the deepest reflector that extends laterally for 100+ m (deepest solid black line in Fig. 7b), the GPR signal is characterized by multiple diffractions (hyperbolic reflections at profile distances between 320 and 400 m, Fig. 7b) or weak laterally continuous reflecting horizons with greater depth (dotted lines in Fig. 7b, profile distances greater than 400 m). We interpret these diffractions to be caused by either boulders (commonly observed on the surface of IDFs, e.g. Fig. 5) or additional crevasses that do not extend to the surface of the IDF. We interpret that the weaker reflecting horizons and the crevasses observed in the layered deposits are produced by the IDF deposits transitioning and flowing into the glacial ice. Consistent with this interpretation, crevasses that imply vertical movement within the fan have been observed at the surface of both the IDFs and valley glaciers during this study and previous surveys (e.g., Kochel and Trop, 2012).

Figure 8 is the full axial GPR profile including the IDF and the glacier at the McCarthy Glacier site (dashed line in Fig. 1). The GPR processing for this GPR profile included time-zero correction, dewow, background subtraction, migration, and elevation correction and is displayed with limited subsurface interpretations. We observe an interface (dotted line in Fig. 8) that is subparallel to the ice surface beginning at a depth of 82 m at the start of the GPR profile and ending at a depth of 45 m at the end of the GPR profile. There are no GPR reflections returning from below this interface, and the thickness of the McCarthy Glacier at the terminus was estimated during GPR data collection to be between 50 m and

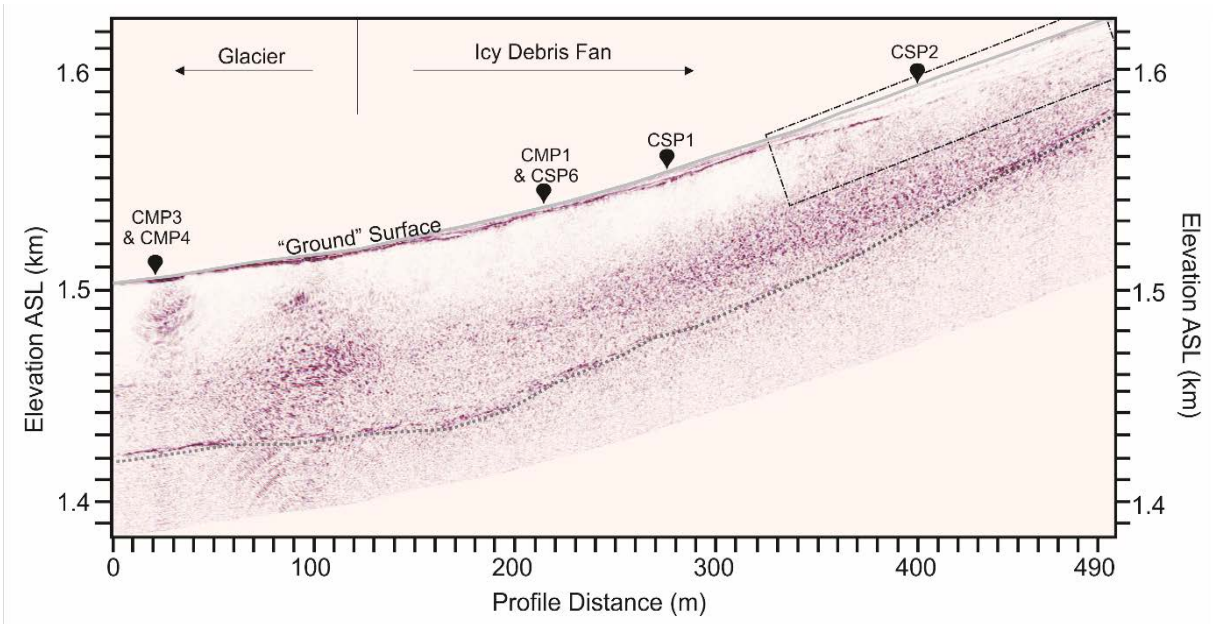

Figure 8. Migrated and elevation-corrected GPR profile extending from glacier (left) up onto mid-fan area (right) collected parallel to the axis of middle fan at McCarthy Glacier extending from the glacier onto the middle IDF (dashed line in Fig. 1). The black rectangle shows the location of the detailed view presented in Figure 7. Elevations from RTK-GPS were used to display ground surface elevations, above sea level (ASL). Migration and depth based on GPR signal velocity of 0.158 m/ns from a reflection at a TWTT of 435 ns on CSP2 (Table 2). The black dotted line connects prominent reflectors at depth interpreted to be the bedrock interface. We interpret a fan thickness of 45 m at mid-fan near CSP2 and a glacier thickness of 82 m.

100 m thick. Thus we interpret this interface to be between the glacial ice / ice derived from IDF deposits above the interface and bedrock below this interface. In addition, the thinning of the IDF in an up-fan direction is consistent with the field relation showing that bedrock is exposed at the apex of the fan.

Conclusions

We have investigated the effect of the antenna polarization, antenna orientation and WARR configuration relative to subsurface reflectors at four IDFs at McCarthy Glacier, Alaska and La Perouse Glacier, New Zealand. Combining the results of WARR soundings and GPR profiles, we have provided an interpretation of the subsurface characteristics of an icy debris fan on the McCarthy Glacier, Alaska.

We conclude that the antenna polarization, TE or TM, did not negatively affect the signal amplitude and thus the identification of reflectors in icy debris fans. In addition, the antenna orientation relative to the axis of the fan, broadside parallel or perpendicular, had a minimal effect on the signal amplitude and thus the GPR reflections observed within the IDFs. We concluded that our data collection procedure could thus collect TE polarization and have the antennas oriented parallel to contours. The WARR configuration – either CMP or CSP – did affect the NMO velocity analysis from a co-located CSP and CMP sounding in addition to the CSP configuration not illuminating a deep reflection.

This conclusion lead us to increasing our survey crew size so that CMP soundings could be collected in GPR surveys after 2013.

The WARR soundings on the IDFs studied here indicate that the GPR signal velocity of these deposits (median NMO velocity of 0.159 m/ns) are similar to velocity estimates from the McCarthy Glacier (median NMO velocity of 0.161 m/ns) as well as other temperate glaciers (Murray et al., 2007). However, we are not interpreting this to mean that the material properties of the icy debris fan are identical to the material properties of a temperate glacier based on the results of this report. We do note that the material properties of a fresh ice avalanche deposit are different than an ablated deposit. Due to suspected dipping interfaces, we could not evaluate GPR signal velocity anisotropy within the IDFs relative to suspected ice flow direction. There did not appear to be GPR signal velocity anisotropy relative to suspected ice flow direction within the McCarthy Glacier.

At McCarthy Glacier, Alaska, the GPR profile on the IDF relative to the subjacent glacier appears to indicate a change in material behavior – brittle in the shallow section and ductile in the deeper section. Although we expect this material change would also lead to a decrease in porosity with depth, there is no consistent change in the NMO velocity with depth in the IDF subsurface from the semblance analysis. It is clear from the GPR profile data that the icy debris fans are heterogeneous, which would produce out-of-plane diffractions or reflections. Hence, a three-dimensional GPR survey would limit complications during interpretation, however, additional survey time is difficult due to the frequent hazards presented on these geomorphically active features.

The GPR data (Fig. 7) reveal changes in the orientation and lateral continuity of the subsurface reflectors, indicating that the IDF deposits on McCarthy Glacier transition with depth and become flowing glacial ice. This observation would indicate that IDFs act as tributaries to the valley glaciers.

Acknowledgements

We thank Keith Williams, Tracey Smith, Erica Rubino, Alex Pellicciotti, Charles Scales and Katherine Wagner for their contributions to this project during either field work or data processing. This research was made possible by funding from National Science Foundation - NSF EAR 1224720. Our early studies were funded by the National Geographic Society – Waitt Foundation Discovery Grant Program and Bucknell Univ. We thank the following parks (and primary contacts) for their support: Alaska – Wrangell-St. Elias National Park and Preserve (M. Loso & E. Veach); New Zealand – New Zealand Dept. of Conservation – Tai Poutini (I. Gruner) and Aoraki National Parks (R. Bellringer). We appreciate the improvements made to this manuscript during reviews leading up to and after the presentation at the IWAGPR 2017 conference. The comments from two reviewers and associated editor are greatly appreciated. We also thank B. Jordan and C. Dill for providing logistical support.

References

Annan, A.P., 2005, Ground Penetrating Radar, Chapter 11 in Near-Surface Geophysics, Volume 13, Butler, D.K. (ed.), SEG Books, 357-438.

Arcone, S.A., 2008, Glaciers and Ice Sheets, Chapter 12 in Ground Penetrating Radar Theory and Applications, Jol, H. M. (ed.), Elsevier Science, 361–388.

Booth, A., Clark, R., and Murray, T., 2010, Semblance response to a ground-penetrating radar wavelet and resulting errors in velocity analysis: Near Surface Geophysics, **8** (3), 235-246.

Bradford, J. H., Harper, J. T., and Brown, J., 2009, Complex dielectric permittivity measurements from ground-penetrating radar data to estimate snow liquid water content in the pendular regime: Water Resources Research, **45** (8), W08403, doi:10.1029/2008WR007341.

Fischer, A., and Kuhn, M., 2013, Ground-penetrating radar measurements of 64 Austrian glaciers between 1995 and 2010. Annals of Glaciology: **54** (64), 179-188.

Jacob, R. W., and Hermance, J. F., 2005, Random and non-random uncertainties in precision GPR measurements: Identifying and compensating for instrument drift: Subsurface Sensing Technologies and Applications, **6** (1), 59-71.

Jacob, R.W. and Urban, T. M., 2016, Ground Penetrating Radar velocity determination and precision estimates using common-midpoint (CMP) collection with hand - picking, semblance analysis and cross-correlation analysis: A case study and tutorial for archaeologists: Archaeometry, **58**, 987–1002, (published online 2015).

Kochel, R.C. and Trop, J.M., 2008, Earth analog for high-latitude landforms and recent flows on Mars: Icy debris fans in the Wrangell volcanic field, Alaska: Icarus, **196**, 63-77.

Kochel, R.C. and Trop, J.M., 2012, Active processes, morphology, and dynamics of icy debris fans: landform evolution along rapidly degrading escarpments in alpine regions undergoing recent deglaciation: Geomorphology, **151-152**, 59-76.

Kochel, R.C., Trop, J.M., and Jacob, R.W., 2018, Geomorphology of icy debris fans: Delivery of ice and sediment to valley glaciers decoupled from icecaps: Geosphere, **14** (4), 1710–1752, supplemental files available. doi: https://doi.org/10.1130/GES01622.1 .

Murray, T., Booth, A., and Rippin, D.M., 2007, Water-content of glacier-ice: limitations on estimates from velocity analysis of surface ground-penetrating radar surveys: Journal of Environmental & Engineering Geophysics, **12** (1), 87-99.

Nobes, D., 1999, The directional dependence of the Ground Penetrating Radar response on the accumulation zones of temperate Alpine glaciers: First Break, **17** (7), 249-259.

Rignot, E., Mouginot, J., Larsen, C. F., Gim, Y., and Kirchner, D., 2013, Low-frequency radar sounding of temperate ice masses in Southern Alaska: Geophysical Research Letters, **40**, 5399–5405, doi: 10.1002/2013GL057452.

Roberts, R.L., and Daniels, J.J., 1996, Analysis of GPR polarization phenomena: Journal of Environmental & Engineering Geophysics, **1** (2), 139–157.

Sensor & Software, Inc., 2015, EKKO Project User Guide. (website: www.sensoft.ca/)

Woodward, J., and Burke, M. J., 2007, Applications of ground-penetrating radar to glacial and frozen materials: Journal of Environmental & Engineering Geophysics, **12** (1), 69-85.